Iron Deposition in the Bone Marrow and Spleen of Nonhuman Primates with Acute Radiation Syndrome

Authors: Day, Regina M., Rittase, W. Bradley, Slaven, John E., Lee, Sang-Ho, Brehm, Grace V., et al.

Source: Radiation Research, 200(6) : 593-600

Published By: Radiation Research Society

URL: https://doi.org/10.1667/RADE-23-00107.1

RADIATION RESEARCH **200**, 593–600 (2023)
0033-7587/23 $15.00

DOI: 10.1667/RADE-23-00107.1

Iron Deposition in the Bone Marrow and Spleen of Nonhuman Primates with Acute Radiation Syndrome

Regina M. Day,[a,1] W. Bradley Rittase,[a] John E. Slaven,[a] Sang-Ho Lee,[b] Grace V. Brehm,[a] Dmitry T. Bradfield,[a] Jeannie M. Muir,[c] Stephen Y. Wise,[a,d] Oluseyi O. Fatanmi,[a,d] Vijay K. Singh[a,d,1]

[a] Division of Radioprotectants, Department of Pharmacology and Molecular Therapeutics, F. Edward Hébert School of Medicine, Uniformed Services University of the Health Sciences, Bethesda, Maryland 20814; [b] Pathology Department, Research Services, Naval Medical Research Center, Silver Spring, Maryland 20910; [c] Department of Pathology, Uniformed Services University of the Health Sciences, Bethesda, Maryland 20814; [d] Armed Forces Radiobiology Research Institute, Uniformed Services University of the Health Sciences, Bethesda, Maryland 20814

Day RM, Rittase WB, Slaven JE, Lee S-H, Brehm GV, Bradfield DT, Muir JM, Wise SY, Fatanmi OO, Singh VK. Iron Deposition in the Bone Marrow and Spleen of Nonhuman Primates with Acute Radiation Syndrome. Radiat Res. 200, 593–600 (2023).

The risk of exposure to high levels of ionizing radiation from nuclear weapons or radiological accidents is an increasing world concern. Partial- or total-body exposure to high doses of radiation is potentially lethal through the induction of acute radiation syndrome (ARS). Hematopoietic cells are sensitive to radiation exposure; white blood cells primarily undergo apoptosis while red blood cells (RBCs) undergo hemolysis. Several laboratories demonstrated that the rapid hemolysis of RBCs results in the release of acellular iron into the blood. We recently demonstrated using a murine model of ARS after total-body irradiation (TBI) and the loss of RBCs, iron accumulated in the bone marrow and spleen, notably between 4–21 days postirradiation. Here, we investigated iron accumulation in the bone marrow and spleens from TBI nonhuman primates (NHPs) using histological stains. We observed trends in increased intracellular and extracellular brown pigmentation in the bone marrow after various doses of radiation, especially after 4–15 days postirradiation, but these differences did not reach significance. We observed a significant increase in Prussian blue-staining intracellular iron deposition in the spleen 13–15 days after 5.8–8.5 Gy of TBI. We observed trends of increased iron in the spleen after 30–60 days postirradiation, with varying doses of radiation, but these differences did not reach significance. The NHP model of ARS confirms our earlier findings in the murine model, showing iron deposition in the bone marrow and spleen after TBI.

[1] Corresponding authors: Vijay K. Singh, Ph.D., email: vijay.singh@usuhs.edu; and Regina M. Day, Ph.D., email: regina.day@usuhs.edu; Division of Radioprotectants, Department of Pharmacology and Molecular Therapeutics, F. Edward Hébert School of Medicine, Uniformed Services University of the Health Sciences, Bethesda, MD, 20814.

INTRODUCTION

Exposure to partial- or total-body high-dose radiation results in potentially fatal multi-organ injuries, collectively known as acute radiation syndrome (ARS) (*1*, *2*). The clinical progression of ARS depends on the tissue-absorbed radiation dose and its distribution within the body. Mild radiation injury in humans can be observed after total-body irradiation (TBI) with as low as ~0.3–0.7, and is characterized by hematopoietic insufficiency, opportunistic infection from immune suppression, and coagulation dysfunction (*1*, *2*). Doses higher than ~3.5–4 Gy can induce hematopoietic acute radiation syndrome (H-ARS) in which hematopoietic progenitors are critically impaired, preventing the regeneration of mature blood cells; mortality can occur within 30 days (*1*, *3–10*). In H-ARS, mature white blood cells (WBC) and many hematopoietic progenitors undergo apoptotic cell death (*6*, *11*). However, reticulocytes and red blood cells (RBCs) lack DNA and apoptotic machinery, and these cells instead undergo hemolysis following radiation exposure (*6*, *12–14*). The destruction of RBCs results in reduced tissue oxygenation and the release of iron, likely contributing to subsequent organ sequelae (*14–19*). Using murine models of H-ARS, our laboratory and others demonstrated increased iron deposition in several tissues, including bone marrow, spleen, heart, and intestines at 1–2 weeks postirradiation (*16–21*). Direct iron assays and/or histological evaluation of the tissue revealed iron increased ~tenfold in the bone marrow and >sixfold in the spleen (*16*, *17*). Increased iron correlated with altered expression of iron binding and transport proteins (*16*, *17*). We also found that increased iron levels in the spleen correlated with markers of ferroptosis, a form of iron-dependent apoptosis (*16*, *17*).

Several animal models have been used to study radiation injury and countermeasure development (*22–24*), but use of the nonhuman primate (NHP) ARS model is preferred for radiation countermeasure approval by the U.S. Food and Drug Administration (*25*). Here, we used archived tissues from previous experiments to investigate iron deposition in the bone marrow, spleen, liver, and heart in NHPs after TBI.

This study is consistent with the principle of the 3Rs (Replace, Reduce, and Refine) in animal research.

MATERIALS AND METHODS

Study Design

As stated above, this study utilized archived tissues from earlier experiments. We collected samples from the following categories of animals: 1. irradiated animals pre-scheduled for euthanasia on a specific day postirradiation without any sign of moribundity (primary objective of studies was mechanistic), 2. moribund animals on various days postirradiation depending on dose of radiation received, 3. irradiated surviving animals euthanized at the end of the study (day 60). We used all animal samples available in our laboratory while accomplishing this study. (See Table 1 footnotes for details of animal groups.)

Animals and Supportive Care

The original protocols for the NHP studies were approved by the Institutional Animal Care and Use Committees [IACUCs: Armed Forces Radiobiology Research Institute (AFRRI) Protocol #2015-12-011, BIOQUAL Inc. Protocol #18-060, and University of Maryland Baltimore Protocol #0581005], and approved by the Department of Defense second tier, Animal Care and Use Review Office. Experiments were performed in strict accordance with the Guide for the Care and Use of Laboratory Animals (*26*). Animals were maintained in facilities accredited by the Association for Assessment and Accreditation of Laboratory Animal Care International. A total of 35 rhesus macaques (*Macaca mulatta*, Chinese sub-strain) were used; 22 were males and 13 were females, 2.5–7 years of age, weighing 3–8 kg (Table 1) (*27*, *28*). Tissues from six healthy animals were used in this study and details of these animals are also provided in Table 1. Prior to the study, all NHPs were quarantined for six weeks. After irradiation, cage-side observations were performed twice daily to score radiation injuries through the experimental endpoints (Table 1) (*28*, *29*). During the 10–20 days postirradiation, animals were scored at least three times a day, no more than 10 h apart. Animals with highly scored criteria and/or blood cell count deficiency were administered additional medical management or euthanized early (*27–29*). Supportive care included administration of antibiotics, rehydration fluids, antipyretics, antidiarrheal agents, analgesics, antiemetics, treatment for mucosal ulcers, and nutritional support (*28*, *29*). Tissues from animals receiving blood transfusions were not included in this study due to potential transfusion-induced red blood cell damage/aging (*30–32*). Euthanasia and euthanasia criteria have been described previously (*29*, *33*).

Irradiation and Dosimetry

Twenty-nine NHPs were irradiated with various doses of ^{60}Co γ-radiation, from sublethal to supralethal doses (4.0, 5.8, 6.0, 6.5, 7.0, 7.2, 8.5 and 12.0 Gy; all 0.6 Gy/min) (*28*, *29*, *34–36*) (Table 1). Food was withheld from animals 12–16 h prior to irradiation to minimize the possibility of vomiting. Approximately 30–45 min before exposure, animals were sedated with 10–15 mg/kg ketamine HCl intramuscularly, placed in Plexiglas boxes, and secured in a seated position. Two NHPs were irradiated simultaneously, oriented back-to-back, using bilateral exposure (*27*, *29*). NHPs were observed throughout the exposure procedure via in-room cameras. Following the radiation exposure, NHPs were returned to their cages where their recovery was monitored.

Photon dosimetry was based on alanine/electron paramagnetic resonance (EPR) which is currently accepted as one of the most precise methods for measuring high radiation doses and is used for comparisons between national metrology institutions (*29*, *37*, *38*). The calibration curves (EMXmicro spectrometer, Bruker Corp., Billerica, MA) for dose measurements at AFRRI are based on standard alanine calibration sets purchased from the U.S. National Institute of Standards and Technology (NIST, Gaithersburg, MD). The alanine dosimeters obtained from NIST were calibrated in terms of absorbed dose to water using the U.S. National Standard Radiation Sources. At AFRRI, identical alanine dosimeters were placed midline within NHP phantoms (Plexiglas cylinders 6.9, 10, 12.5 cm in diameter and 34.5 cm length) and irradiated to approximately 100 Gy. Measurement of their EPR signals using the calibration curve constructed with alanine dosimeters from NIST-provided dose rates to water in the core bodies of NHP. Doses were delivered to midline tissues. To deliver the accurate dose, abdominal widths were measured with digital calipers. A correction was applied for the difference in mass energy absorption coefficients between water and soft tissue.

TABLE 1
Nonhuman Primate Groups and Sample Collections

Animal ID[1]	Sex	Age (year)	Radiation dose (Gy)	Euthanasia[2] (days)
RA1240M	M	4.9	0	-
RA1319M	M	5.3	0	-
RA0589M	M	4.2	0	-
14041532F	F	6.4	0	-
RA1251M	M	5.0	0	-
TEST-NHP	F	Unknown	0	-
RA2695M	M	4.8	4.0	30[3]
RA3228F	F	4.1	4.0	30[3]
1606069M	M	3.7	4.0	30[3]
1608010F	F	3.5	4.0	30[3]
1608016F	F	3.5	5.8	21
1607030F	F	3.6	5.8	22
1608039M	M	3.5	5.8	30[3]
1603015M	M	3.9	5.8	30[3]
RA0521F	F	4.9	6.0	13
RA2654F	F	4.1	6.5	60[4]
RA2705M	M	5.3	6.5	15
RA2708M	M	4.3	6.5	60[4]
RA2796M	M	4.3	6.5	60[4]
RA2698M	M	4.2	6.5	60[4]
RA0550M	M	5.3	7.2	60[4]
RA1991M	M	4.0	7.2	60[4]
RA1377M	M	4.5	7.2	60[4]
RA0580M	M	6.2	7.2	60[4]
RA1956M	M	4.3	7.6	60[4]
RA1988M	M	4.0	7.6	60[4]
RA2318M	M	5.1	8.5	15
RA2692M	M	4.9	12.0	4[3]
RA2892M	M	3.7	12.0	4[3]
RA2619F	F	5.0	12.0	4[3]
RA2922F	F	4.2	12.0	7
RA3238F	F	3.8	12.0	7
RA2931M	M	4.2	12.0	7
RA3291F	F	3.9	12.0	7
RA2378F	F	5.0	12.0	7

[1] Animal number; [2] day of euthanasia after irradiation; [3] day of prescheduled after irradiation euthanasia without any sign of moribundity; [4] surviving animals euthanized at the end of the study (day 60). The remaining animals were moribund and were euthanized on various days as a result of radiation exposure. F = female; M = male.

Tissue Sample Collection and Histopathology

Sternums, spleens, hearts, and livers were obtained at necropsy, either at early euthanasia time points or at the experimental endpoint. The middle sternebrae of the sternum, excluding the upper and lower processes, was fixed in 10% zinc-buffered formalin for analysis.

Paraffin embedding, sectioning, and staining [hematoxylin and eosin (H&E) or Prussian blue] were performed by Histoserv, Inc. (Germantown, MD). Digital images were obtained with a Zeiss Axioscan slide scanner with Zeiss Zen software (Carl Zeiss Meditech, Inc., Dublin, CA). An Olympus IX73 microscope (Olympus, Center Valley, PA) was used for 40× magnification. ImageJ software (NIH, Bethesda, MD; https://imagej.nih.gov/ij/-download.html) was used for histological image analysis for quantification (*17*). Hemosiderin was expressed as a percentage of area in sections counterstained with nuclear fast red. For Prussian blue, images were divided into grids of 100 boxes and a random number generator was used to select three boxes to quantify blue area. Histological and morphometric analyses, and white pulp changes after irradiation were evaluated by a board-certified veterinary pathologist blinded to treatment groups. Percentage of hematopoietic cells to adipocytes in the bone marrow was determined by a board-certified hematological pathologist blinded to the treatment groups.

Statistical Analysis

Euthanasia for the NHP early time points was performed if morbidity was identified. For analysis, data was grouped as closely as possible into time points for 1, 2, 3–4 weeks, and 60 days postirradiation. The 60-day samples were sub-grouped into 4.0–6.5 Gy and 7.2–7.6 Gy. Data was analyzed using two tailed ANOVA with Dunnett's T3 multiple comparisons test using GraphPad Prism V6 (GraphPad Prism Software, Inc., San Diego, CA). A P value <0.05 was considered significant.

RESULTS

Effect of TBI on Bone Marrow Cellularity and Iron Deposition

Our previous studies showed increased iron deposition in murine bone marrow after TBI (*16*). In unirradiated control NHPs, the bone marrow sections showed the presence of lymphoid and myeloid hematopoietic precursor cells with larger oval to round nuclei with mildly clumped chromatin materials (Fig. 1A). In the normal bone marrow sections, cellularity was ~1:4 ratio of adipocytes to hematopoietic cells and precursors. Interestingly, at day 30 postirradiation, the bone marrow after 4 Gy TBI (sublethal dose) appeared histologically almost normal, with ~3:7 adipocytes to hematopoietic cells (Fig. 1B).

Higher doses of radiation induced greater losses of normal bone marrow cellularity. After exposure to 6.0–8.5 Gy from 13–15 days postirradiation, there was diffuse arrangement of hematopoietic precursors, with increased adipocytes in animals euthanized at early time points (Fig. 1C). At these early euthanasia time points, the bone marrow was characterized by marked to severe cellular aplasia, with loss of all precursor cell lineages. Only minimal numbers of mature myeloid cells (neutrophils and mononuclear cells) persisted in isolated areas of the bone marrow that displayed increased adipocytes. The venules lined by endothelial cells within the bone marrow remained intact in this period. By 20 days postirradiation, there was early regenerative process that included erythrocytic precursors with small dark, round nuclei. Other precursor types were also present, with round to oval pale-staining nuclei with coarsely stippled nuclear chromatin patterns. These cells were about twice as large as erythrocytes, with abundant eosinophilic cytoplasm, and arranged mostly in aggregates. In these higher-dose radiation groups, animals that survived 30 days postirradiation exhibited mild to moderate cellular proliferation, characterized by a mixture of hematopoietic precursor cells including moderate levels of megakaryocyte precursors.

In contrast to exposure with other radiation doses, exposure to 12 Gy (supralethal dose) resulted in almost complete loss of normal cellularity, and the animals were euthanized 4–7 days after irradiation (Fig. 1D). Only minimal numbers of mature myeloid cells, mostly neutrophils and mononuclear cells, persisted in some isolated areas of the bone marrow, which otherwise consisted of a network of adipocytes. Interestingly, the venules lined by endothelial cells within the bone marrow appeared to remain intact.

Quantification of bone marrow cellularity showed dose-dependent and time-dependent loss of hematopoietic cellularity in the bone marrow (Fig. 1E and Supplementary Table S1;[2] https://doi.org/10.1667/RADE-23-00107.1.S1). In animals euthanized at early endpoints between 13–15 days postirradiation, 5.8–8.5 Gy resulted in ~95% loss of bone marrow cellularity ($P = 0.002$). Interestingly, by 21–30 days after irradiation with 4.0–5.8 Gy, bone marrow cellularity was ~1.3% ($P = 0.047$). By 60 days after exposure to either 4.0–6.5 or 7.2–7.6 Gy, the bone marrow cellularity was close to baseline levels ($P = 0.93$ and 0.17, respectively; statistics shown in Supplementary Table S1). At 4–7 days after 12 Gy irradiation, the bone marrow exhibited only 9% cellularity ($P = 0.0007$, Supplementary Table S1).

We previously demonstrated the deposition of ferric iron (Fe^{3+}) in histological sections of murine sternebrae after TBI using Prussian blue staining (*16*). However, the NHP sternebrae are composed of much thicker cancellous bone than murine sternebrae, requiring an extended period for the decalcification process, resulting in a loss of capacity for Prussian blue staining. Intracellular brown pigment was observed that superimposed with the nuclear fast red counter-stained cellular structures in the NHP bone marrow; we hypothesized that this may be iron-bound hemosiderin. Additionally, extracellular brown pigment was also observed which could be iron-free hematoidin. Total brown stain was quantified (Fig. 1F, statistics, Supplementary Table S2; https://doi.org/10.1667/RADE-23-00107.1.S1). Although we detected a trend toward increased brown pigment in the NHP bone marrow at 13–15 days in the 5.8–8.5 Gy groups and at 4–7 days in the 12 Gy TBI groups, none of the groups displayed a significant increase compared with control levels (Supplementary Table S2).

Effect of TBI on Iron Deposition in the Spleen

We previously demonstrated using the murine model of ARS that significant levels of iron are deposited in the spleen, with maximal levels at ~7–14 days postirradiation (*17*). In unirradiated NHPs, the normal spleen sections were characterized by prominent white pulp with a distinct central germinal center surrounded by a thin dark layer of mantle zone, further surrounded by the marginal zone (Fig. 2A). Animals subjected

[2] Editor's note. The online version of this article (DOI: https://doi.org/10.1667/RADE-23-00107.1) contains supplementary information that is available to all authorized users.

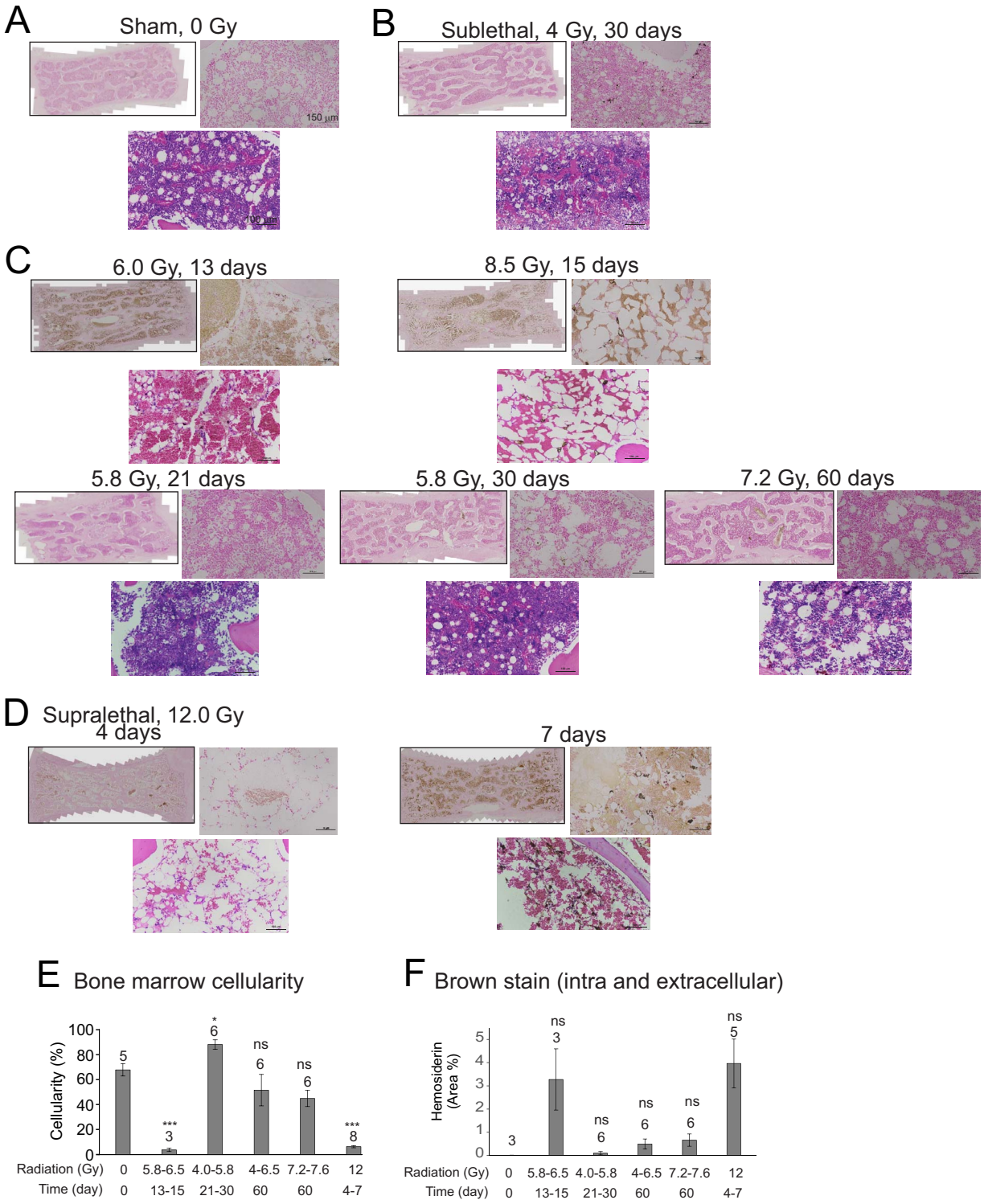

FIG. 1. Effect of irradiation on brown pigmentation in the bone marrow in NHPs. Sternums were obtained from NHPs at the indicated times of euthanasia after exposure to various doses of radiation. Sternums stained with Prussian blue with fast red counterstain (upper images, full slide images and 20× magnification), or with H&E allowing visualization of cellularity (lower images, 30× magnification). Representative images are shown. Panel A: Sham irradiation (0 Gy); Panel B: Sublethal irradiation, 4 Gy, 30 days; Panel C: 5.8–8.5 Gy, 13–60 days; Panel D: Supralethal irradiation, 12 Gy, 4–7 days; Panel E: Quantification of bone marrow cellularity. Bone marrow cellularity in sternums was quantified by a hematological pathologist blinded to the treatment groups; Panel F: Quantification of bone marrow brown pigmentation. Bars indicate means per group ± SEM. The number above each bar indicates the n per group. *$P < 0.05$ compared with control group. ***$P < 0.001$ and ns indicates not significant compared with control.

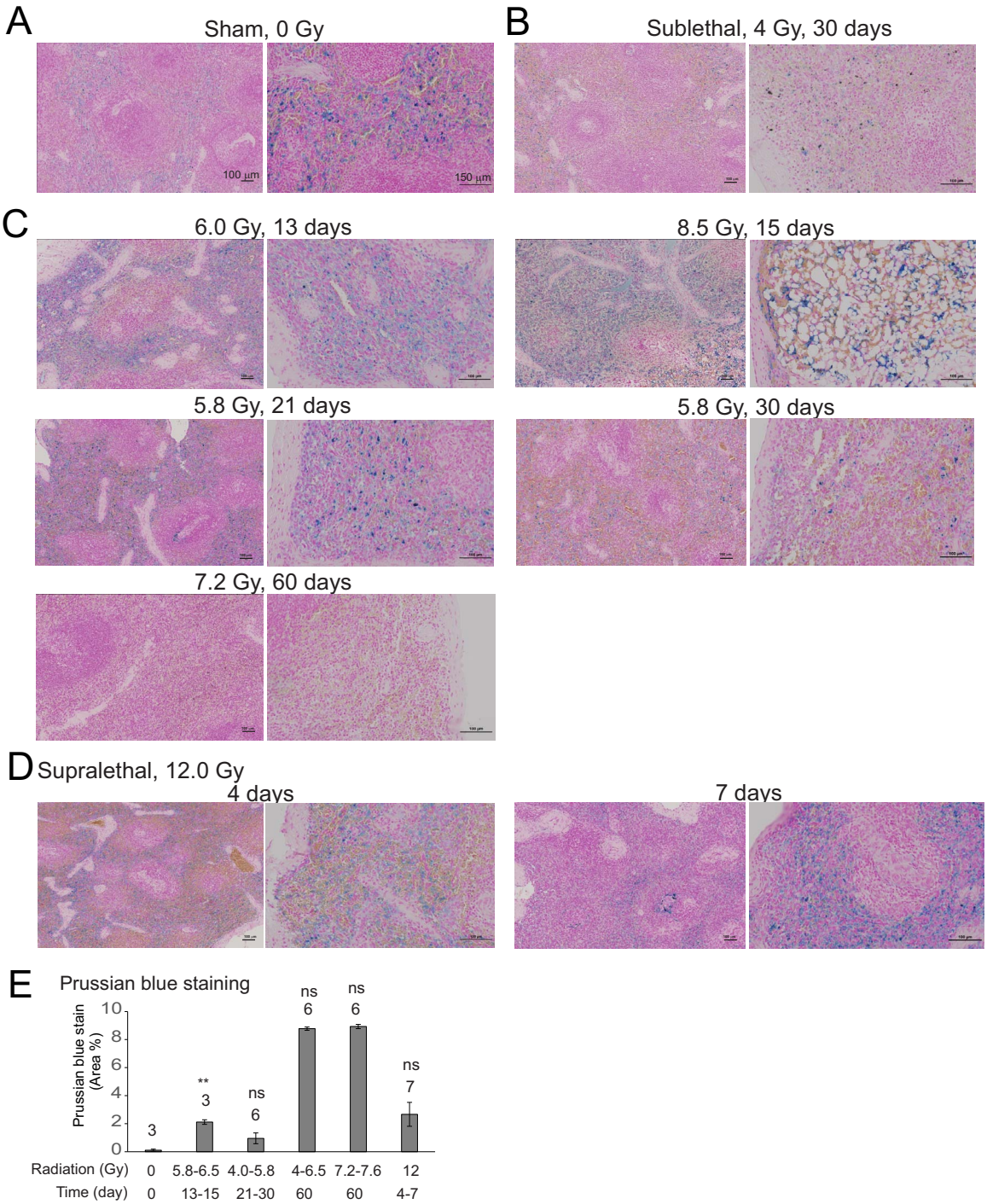

FIG. 2. Effect of irradiation on iron deposition in the spleen in NHPs. Spleen tissue was obtained from NHPs at the indicated times of euthanasia after exposure to various doses of radiation. Fixed tissues were stained with Prussian blue; images show 10× and 30× magnification. Panel A: Sham irradiation (0 Gy); Panel B: Sublethal irradiation, 4 Gy, 30 days; Panel C: 5.8–8.5 Gy, 13–60 days; Panel D: Supralethal irradiation, 12 Gy, 4–7 days; Panel E: Quantification of spleen Prussian blue staining. Blue staining was quantified using random fields (see Methods). Bars indicate means per group ± SEM. The number of animals in each group is indicated above each bar. ** $P < 0.01$ and ns indicates not significant compared with control.

to 4 Gy TBI showed only moderate cellular loss, and the white pulp showed nearly normal morphology at the experimental endpoint of 30 days postirradiation (Fig. 2B). Animals subjected to 5.8 Gy TBI showed slightly more cellular loss at all time points, especially within the white pulp (Fig. 2C). In animals subjected to 6.0 Gy or higher TBI that were euthanized early, marked to severe white pulp cellular losses were apparent. The white pulp of these spleens were characterized by thin to very thin peripheral layers of lymphocytes (Fig. 2C and D). In animals that survived 7.2 Gy TBI to the 60 day

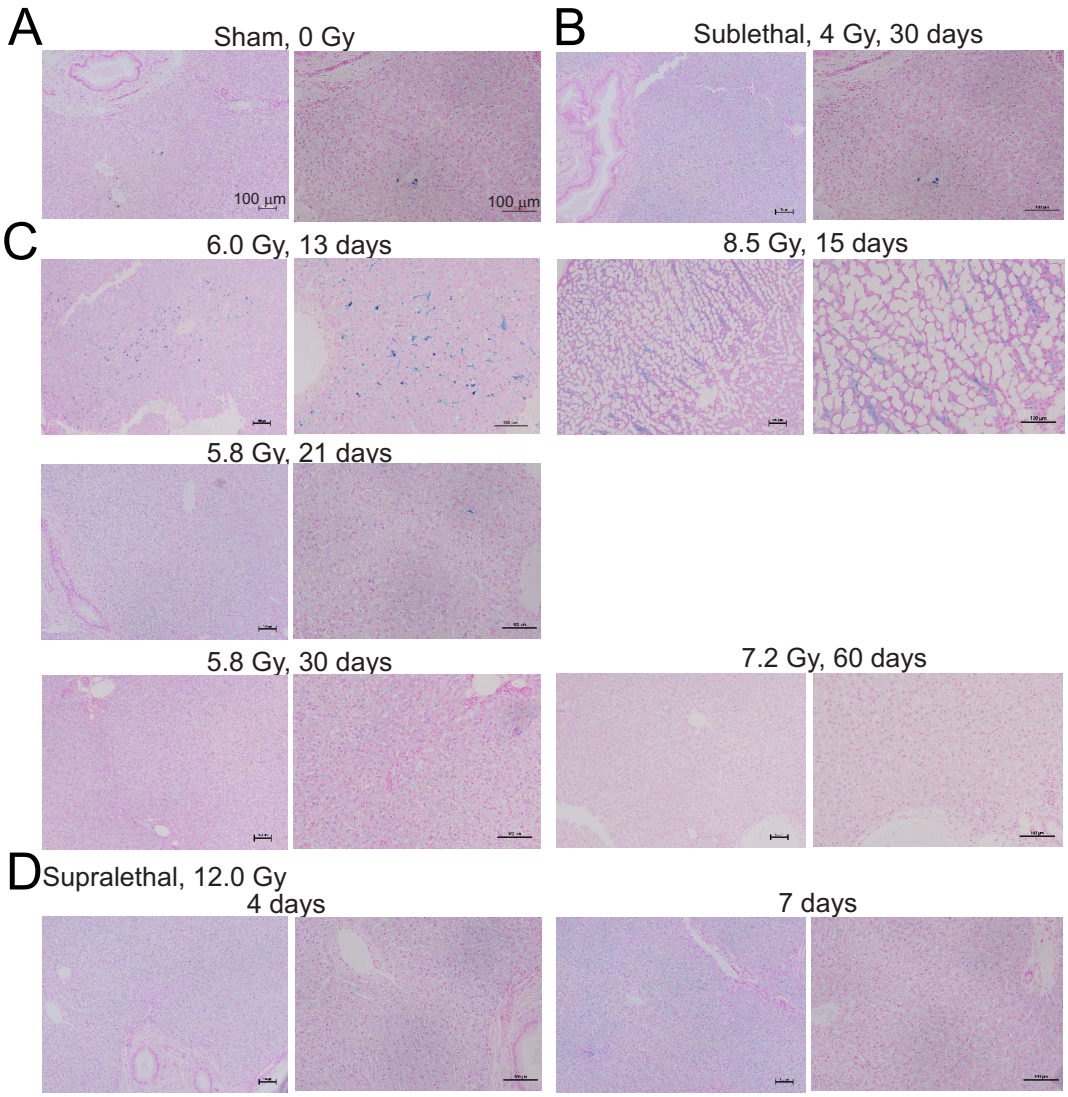

FIG. 3. Effect of irradiation on iron deposition in the liver in NHPs. Liver tissue was obtained from NHPs at the indicated times of euthanasia after exposure to various doses of radiation. Fixed tissues were stained with Prussian blue; representative images show 10× and 20× magnification. Panel A: Sham irradiation (0 Gy); Panel B: Sublethal irradiation, 4 Gy, 30 days; Panel C: 5.8–8.5 Gy, 13–60 days; Panel D: Supralethal irradiation, 12 Gy, 4–7 days.

experimental endpoint, there was only mild to minimal reduction of white pulp cellular components, suggesting a recovery of normal cellularity (Fig. 2C and D). These tissue sections evaluated are characterized by distinct white pulp morphology with germinal centers surrounded by a peripheral zone composed of lymphocytes.

In unirradiated NHP spleen tissues, a low level of Prussian blue staining was present (Fig. 2A), consistent with the normal spleen function for iron recycling. In spleen tissue sections taken from animals 2 weeks after they were exposed to 5.8–6.5 Gy, there was a significant increase in Prussian blue staining, localized to red pulp areas ($P = 0.01$) (Fig. 2E, statistics, Supplementary Table S3; https://doi.org/10.1667/RADE-23-00107.1.S1). This finding was expected given that erythrocyte extravascular removal occurs via phagocytosis in the red pulp by macrophages. There were trends toward increased Prussian blue staining after 60 days in both 4.0–5.8 Gy and 7.2–7.6 Gy groups and at 4–7 days in the 12 Gy irradiated group, but these did not reach significance (Supplementary Table S3). We noted that extracellular brown pigment was observed in the spleen, which could also be hematoidin.

Effect of TBI on Iron Deposition in the Liver and Heart

We previously showed increased hemosiderin in the liver in a murine model of TBI (*16*). None of the livers showed structural pathologies, however there were minimal to mild increases in the blue Fe^{3+} staining affecting macrophages, Kupfer cells, and lining the hepatic sinusoids that separate hepatic cords in some sections (Fig. 3). We interpret this as resident cells from the liver removing damaged erythrocytes from circulation following TBI. In the group irradiated with 8.5 Gy, after 15 days, in the liver we identified extensive adipocyte expansion (Fig. 3C).

DISCUSSION

There is currently an increasing concern worldwide regarding potential radiation exposures, whether from clinical uses of radiation, nuclear accidents, or military/terrorist events, emphasizing the need for radiation countermeasure development (*39–42*). Importantly, the development of effective countermeasures requires a complete understanding of the mechanisms of radiation-induced sequelae (*17*, *39–42*). Although the immediate effects of ionizing radiation exposure are believed to be due to direct effects on cells and oxygen and nitrogen radical generation, the mechanism(s) of development of late effects after radiation exposure are not completely understood. Our laboratory and others demonstrated, using mice, that radiation-induced RBC hemolysis causes the release of iron which can then be found in bone marrow, spleen, liver, heart, and intestinal tissues (*16–21*). Our laboratory and others also showed that the elevated iron after irradiation may be associated with tissue dysfunction and ferroptosis (*17*, *18*, *20*, *21*).

Here we demonstrated intracellular and extracellular brown pigmentation in the bone marrow and increased Prussian blue- iron staining in the spleen in an NHP model of ARS. We also observed low levels of Prussian blue staining in NHP livers after TBI. The possible presence of iron-free hematoidin in the bone marrow and spleens of NHPs suggests that free iron may be released after radiation-induced cell damage; the extracellular pigmentation requires further investigation (*43*). These data are consistent with our previous findings in the murine model, suggesting that iron tissue deposition is not limited to the murine model (*16*, *17*). Increased hemosiderin and possibly the formation of iron-free hematoidin were observed in NHP exposed to a wide range of radiation doses. Improved understanding of the mechanisms of both the immediate injuries resulting from radiation exposure, as well as the mechanisms of indirect radiation injuries will allow the development of radiation medical countermeasures with multiple mechanisms of action to prevent and mitigate radiation injuries.

ACKNOWLEDGMENTS

The authors thank the staff members of AFRRI Radiation Source Department for supporting NHP irradiation and the Veterinary Science Department for NHP care during animal experimentation. For some of the authors, this work was prepared as part of their official duties as employees of the U.S. Government. Under Title 17 U.S.C. §105, copyright protection is not available for any work of the United States Government. According to Title 17 U.S.C §101, this included work prepared by employees of the U.S. Government or members of the military. The views in this article are those of the authors and are not necessarily the views, policies, or positions of the Uniformed Services University of the Health Sciences, the Armed Forces Radiobiology Research Institute, Department of the Navy, Department of Defense, or the U.S. Federal Government. This work was supported by the CDMRP (W81XWH-15-C-0117, JW140032), NIAID (AAI12044-001-07000, Work plan G) as a part of an Interagency-Agreement and USUHS/AFRRI (grant # AFR-B4-10978) to VKS and by the Defense Medical Research and Development Program (DMRDP) grant VP000264-01 to RMD.

Received: May 24, 2023; accepted: October 23, 2023; published online: November 16, 2023

REFERENCES

1. Garau MM, Calduch AL, Lopez EC. Radiobiology of the acute radiation syndrome. Rep Pract Oncol Radiother 2011; 16:123-30.
2. Acute radiation syndrome: A fact sheet for clinicians. Radiation Emergencies 2018. Available at: https://www.cdc.gov/nceh/radiation/emergencies/arsphysicianfactsheet.htm [Last accessed 2022].
3. Kennedy AR, Maity A, Sanzari JK. A review of radiation-induced coagulopathy and new findings to support potential prevention strategies and treatments. Radiat Res 2016; 186:121-40.
4. Wagemaker G. Heterogeneity of radiation sensitivity of hemopoietic stem cell subsets. Stem Cells 1995; 13 Suppl 1:257-60.
5. Singh VK, Romaine PL, Newman VL, Seed TM. Medical countermeasures for unwanted CBRN exposures: part II radiological and nuclear threats with review of recent countermeasure patents. Expert Opin Ther Pat 2016; 26:1399-408.
6. Peslak SA, Wenger J, Bemis JC, Kingsley PD, Frame JM, Koniski AD, et al. Sublethal radiation injury uncovers a functional transition during erythroid maturation. Exp Hematol 2011; 39:434-45.
7. Dorr H, Meineke V. Acute radiation syndrome caused by accidental radiation exposure-therapeutic principles. BMC Med 2011; 9:126.
8. Anno GH, Young RW, Bloom RM, Mercier JR. Dose response relationships for acute ionizing-radiation lethality. Health Phys 2003; 84:565-75.
9. McCann DGC. Radiation poisoning: Current concepts in the acute radiation syndrome. Am J Clin Med 2006; 3:13-21.
10. Armed Forces Radiobiology Research Institute. Medical Management of Radiological Casualities. Fourth ed. Bethesda, MD, USA: Armed Forces Radiobiology Research Institute; 2013.
11. Cheki M, Shirazi A, Mahmoudzadeh A, Bazzaz JT, Hosseinimehr SJ. The radioprotective effect of metformin against cytotoxicity and genotoxicity induced by ionizing radiation in cultured human blood lymphocytes. Mutat Res 2016; 809:24-32.
12. Puchala M, Szweda-Lewandowska Z, Kiefer J. The influence of radiation quality on radiation-induced hemolysis and hemoglobin oxidation of human erythrocytes. J Radiat Res 2004; 45:275-9.
13. Zhang B, Liu B, Zhang H, Wang J. Erythrocyte stiffness during morphological remodeling induced by carbon ion radiation. PLoS One 2014; 9:e112624.
14. Zhang XH, Lou ZC, Wang AL, Hu XD, Zhang HQ. Development of serum iron as a biological dosimeter in mice. Radiat Res 2013; 179:684-9.
15. Xie L-H, Zhang X-H, Hu X-D, Min X-Y, Zhou Q-F, Zhang H-Q. Mechanisms of an increased level of serum iron in gamma-irradiated mice. Radiat Environ Biophys 2016; 55:81-8.
16. Rittase WB, Muir JM, Slaven JE, Bouten RM, Bylicky MA, Wilkins WL, et al. Deposition of iron in the bone marrow of a murine model of hematopoietic acute radiation syndrome. Exp Hematol 2020; 84:54-66.
17. Rittase WB, Slaven JE, Suzuki YJ, Muir JM, Lee S-H, Rusnak M, et al. Iron deposition and ferroptosis in the spleen in a murine model of acute radiation syndrome. Int J Mol Sci 2022; 23:11029.
18. Zhang J, Zheng L, Wang Z, Hailong P, Hu W, Nie J, et al. Lowering iron levels protects against bone loss in focally irradiated and contralateral femurs through distinct mechanisms. Bone 2019; 120:50-60.
19. Zhang F, Liu T, Huang HC, Zhao YY, He M, Yuan W, et al. Activation of pyroptosis and ferroptosis is involved in radiation-induced intestinal injury in mice. Biochem Biophys Res Commun 2022; 631:102-9.
20. Zhang X, Xing X, Liu H, Feng J, Tian M, Chang S, et al. Ionizing radiation induces ferroptosis in granulocyte-macrophage

hematopoietic progenitor cells of murine bone marrow. Int J Radiat Biol 2020; 96:1-12.

21. Miller SJ, Chittajallu S, Sampson C, Fisher A, Unthank JL, Orschell CM. A potential role for excess tissue iron in development of cardiovascular delayed effects of acute radiation exposure. Health Phys 2020; 119:659-65.
22. Williams JP, Brown SL, Georges GE, Hauer-Jensen M, Hill RP, Huser AK, et al. Animal models for medical countermeasures to radiation exposure. Radiat Res 2010; 173:557-78.
23. Singh VK, Newman VL, Berg AN, MacVittie TJ. Animal models for acute radiation syndrome drug discovery. Expert Opin Drug Discov 2015; 10:497-517.
24. Singh VK, Olabisi AO. Nonhuman primates as models for the discovery and development of radiation countermeasures. Expert Opin Drug Discov 2017; 12:695-709.
25. U.S. Food and Drug Administration. Guidance document: Product development under the Animal Rule. 2015. Available at: http://www.fda.gov/downloads/drugs/guidancecomplianceregulatoryinformation/guidances/ucm399217.pdf [Last accessed 2022].
26. National Research Council of the National Academy of Sciences. Guide for the Care and Use of Laboratory Animals. 8th ed. Washington, DC: National Academies Press; 2011.
27. Cheema AK, Li Y, Moulton J, Girgis M, Wise SY, Carpenter A, et al. Identification of novel biomarkers for acute radiation injury using multiomics approach and nonhuman primate model. Int J Radiat Oncol Biol Phys 2022; 114:310-20.
28. Garg S, Garg TK, Wise SY, Fatanmi OO, Miousse IR, Savenka AV, et al. Effects of gamma-tocotrienol on intestinal injury in a GI-specific acute radiation syndrome model in nonhuman primate. Int J Mol Sci 2022; 23.
29. Singh VK, Kulkarni S, Fatanmi OO, Wise SY, Newman VL, Romaine PL, et al. Radioprotective efficacy of gamma-tocotrienol in nonhuman primates. Radiat Res 2016; 185:285-98.
30. Schaid TR, Jr., Cohen MJ, D'Alessandro A, Silliman CC, Moore EE, Sauaia A, et al. Trauma induces intravascular hemolysis, exacerbated by red blood cell transfusion and associated with disrupted arginine-nitric oxide metabolism. Shock 2023; 59:12-9.
31. Bush K, Shea L, San Roman J, Pailloz E, Gaughan J, Porter J, et al. Whole blood in trauma resuscitation: What is the real cost? J Surg Res 2022; 275:155-60.
32. Hasan RA, Asif M, Tuott EE, Stansbury LG, Hess JR. Rates of delayed hemolytic transfusion reactions observed in a trauma center. Transfusion 2021; 61:2035-40.
33. Li Y, Singh J, Varghese R, Zhang Y, Fatanmi OO, Cheema AK, et al. Transcriptome of rhesus macaque (Macaca mulatta) exposed to total-body irradiation. Sci Rep 2021; 11:6295.
34. Vellichirammal NN, Sethi S, Pandey S, Singh J, Wise SY, Carpenter AD, et al. Lung transcriptome of nonhuman primates exposed to total- and partial-body irradiation. Mol Ther Nucleic Acids 2022; 29:584-98.
35. Garg TK, Garg S, Miousse IR, Wise SY, Carpenter AD, Fatanmi OO, et al. Gamma-tocotrienol modulates total-body irradiation-induced hematopoietic injury in a nonhuman primate model. Int J Mol Sci 2022; 23:16170.
36. Vellichirammal NN, Sethi S, Avuthu N, Wise SY, Carpenter AD, Fatanmi OO, et al. Transcriptome profile changes in the jejunum of nonhuman primates exposed to supralethal dose of total- or partial-body radiation. BMC Genomics 2023; 24:274.
37. Nagy V. Accuracy considerations in EPR dosimetry. Appl Radiat Isot 2000; 52:1039-50.
38. International Standardization Organization and ASTM International. Standard Practice for Use of an Alanine-EPR Dosimetry System. Geneva, Switzerland: ASTM International, ISO and West Conshohocken (US:PA); 2013. p. 7.
39. Hofer M, Hoferova Z, Falk M. Pharmacological modulation of radiation damage. Does It exist a chance for other substances than hematopoietic growth factors and cytokines? Int J Mol Sci 2017; 18:1385.
40. Russ E, Davis CM, Slaven JE, Bradfield DT, Selwyn RG, Day RM. Comparison of the medical uses and cellular effects of high and low linear energy transfer radiation. Toxics 2022; 10:628.
41. Singh VK, Seed TM. Radiation countermeasures for hematopoietic acute radiation syndrome: growth factors, cytokines and beyond. Int J Radiat Biol 2021; 97:1526-47.
42. Hofer M, Hoferova Z, Depes D, Falk M. Combining pharmacological countermeasures to attenuate the acute radiation syndrome-A concise review. Molecules 2017; 22:834.
43. Fernandez-Flores, A. Two new forms of hematoidin in the skin. J Cutan Path 2015; 42:1026-30.